Reduction Kinetics of Wüstite Scale on Pure Iron and Steel Sheets in Ar and H_2 Gas Mixture

WEICHEN MAO and WILLEM G. SLOOF

A dense and closed Wüstite scale is formed on pure iron and Mn alloyed steel after oxidation in Ar + 33 vol pct CO_2 + 17 vol pct CO gas mixture. Reducing the Wüstite scale in Ar + H_2 gas mixture forms a dense and uniform iron layer on top of the remaining Wüstite scale, which separates the unreduced scale from the gas mixture. The reduction of Wüstite is controlled by the bulk diffusion of dissolved oxygen in the formed iron layer and follows parabolic growth rate law. The reduction kinetics of Wüstite formed on pure iron and on Mn alloyed steel are the same. The parabolic rate constant of Wüstite reduction obeys an Arrhenius relation with an activation energy of 104 kJ/mol if the formed iron layer is in the ferrite phase. However, at 1223 K (950 °C) the parabolic rate constant of Wüstite reduction drops due to the phase transformation of the iron layer from ferrite to austenite. The effect of oxygen partial pressure on the parabolic rate constant of Wüstite reduction is negligible when reducing in a gas mixture with a dew point below 283 K (10 °C). During oxidation of the Mn alloyed steel, Mn is dissolved in the Wüstite scale. Subsequently, during reduction of the Wüstite layer, Mn diffuses into the unreduced Wüstite. Ultimately, an oxide-free iron layer is obtained at the surface of the Mn alloyed steel, which is beneficial for coating application.

DOI: 10.1007/s11663-017-1037-2

I. INTRODUCTION

ADVANCED high strength steels (AHSS) are used in automotive industries to reduce the weight of car bodies thereby reducing fuel consumption and CO_2 emissions.[1] To protect AHSS against corrosion, a zinc coating is usually applied to the surface by hot-dip galvanizing.[2] During the hot-dip galvanizing process, the steel strip passes through continuous annealing furnaces before entering the zinc bath. The final annealing atmosphere is usually a gas mixture of N_2 and H_2 with some water vapor. However, the alloying elements in AHSS, such as Mn, Si, Cr, Al *etc*., can form stable oxides during this annealing process prior to galvanizing. These alloying element oxides at the steel surface lower the zinc wettability[3] and hence degrade the quality of the galvanized steel product.[4] One approach to mitigate the formation of external oxides during annealing is by annealing at high dew points to promote internal oxidation of alloying elements.[5] However, alloying element oxides can still be observed at the steel surface after annealing at high dew points, even when the annealing conditions favor internal oxidation.[6] An alternative way to create an oxide-free steel surface during annealing prior to galvanizing is by first forming a uniform thin $Fe_{1-\delta}O$ (Wüstite) layer at the steel surface that subsequently is reduced into iron.[7] Then the unreduced alloying element oxides are buried underneath the steel surface.

Generally, the reduction process of Wüstite goes through three different stages.[8] First oxygen of the Wüstite reacts with H_2 at the very surface.[9] Depending on the oxygen partial pressure, Wüstite can accommodate cation vacancies with a relatively large concentration (iron deficiency can reach up to 10 pct.[10]) However, if the concentration of cation vacancies in the bulk Wüstite before reduction is higher than the equilibrium cation vacancy concentration, the initial reduction of Wüstite only decreases the amount of cation vacancies instead of forming metallic iron.[11] This decrease of concentration of cation vacancies at the Wüstite surface leads to an outward flux of these vacancies.[12] Next, when the surface concentration of oxygen drops below the value given by the Wüstite/iron phase boundary, iron nucleates and grow laterally at the surface.[8,11] Eventually, iron covers the whole surface. Then, the iron layer separates the Wüstite from the

WEICHEN MAOL is with the Materials Innovation Institute (M2i), Elektronicaweg 25, 2628 XG, Delft, The Netherlands, and also with the Department of Materials Science and Engineering, Delft University of Technology, Mekelweg 2, 2628 CD, Delft, The Netherlands. Contact e-mail: W.Mao@tudelft.nl WILLEM G. SLOOF is with the Department of Materials Science and Engineering, Delft University of Technology, Mekelweg 2, 2628 CD, Delft, The Netherlands.

Manuscript submitted February 7, 2017.
Article published online July 12, 2017.

reduction atmosphere. Subsequently, the Wüstite reduction proceeds by oxygen diffusion through the iron layer formed at the surface.[13] This stage is referred to as the steady-state reduction of Wüstite.

The kinetics of Wüstite reduction during the three stages are different. The rate of oxygen removal by hydrogen at Wüstite surface in the first stage of reduction as well as the lateral growth rate of iron nuclei during the second stage have been studied in detail.[8,9,14,15] However, a detailed description of the kinetics of Wüstite reduction in the third stage, *i.e.*, by oxygen diffusion through the occurring dense iron layer, is lacking.[16] First a model will be presented to predict the reduction kinetics of Wüstite quantitatively. Next, the reduction kinetics of a Wüstite scale formed on pure iron and Mn alloyed steel sheet is studied experimentally at different annealing temperatures in the Ar + H_2 atmosphere with different hydrogen partial pressures and dew points. Finally, the composition and microstructure of the surface are analyzed.

II. KINETICS OF STEADY-STATE WÜSTITE REDUCTION

The kinetics of steady-state reduction of Wüstite has been described in References 13 and 17 only qualitatively. In this paper, however, the kinetics of steady-state reduction of Wüstite is quantified. It is assumed that a closed and dense Fe layer is formed at the surface that separates the $Fe_{1-\delta}O$ scale from the reducing gas atmosphere; see Figure 1.

At the interface between the formed iron layer and the remaining Wüstite layer ($Fe/Fe_{1-\delta}O$), the Wüstite decomposes into iron and oxygen according to:

$$Fe_{1-\delta}O = (1-\delta)Fe + \underline{O},$$

in which $\underline{O}$ denotes the oxygen atom dissolved in the formed iron layer as mobile solid solute without any charges. Then the dissolved oxygen diffuses through the reduced iron layer and reacts with the hydrogen at the gas/iron interface. Ultimately, the diffusion of dissolved oxygen across the iron layer governs the rate of Wüstite reduction, and local thermodynamic equilibrium is established at both $Fe/Fe_{1-\delta}O$ and gas/Fe interfaces. This implies that the reactions at these interfaces and the transport of species in the gas phase are fast compared with the diffusion of species in the iron layer. Also, the oxygen activity is considered to be constant across the remaining Wüstite scale and equals the dissociation oxygen partial pressure of $Fe_{1-\delta}O$. Hence, the iron deficiency δ (*i.e.*, the concentration of cation vacancies) in the $Fe_{1-\delta}O$ scale remains constant during reduction process. The concentration of dissolved oxygen in Fe at the surface is determined by the oxygen partial pressure in the gas phase through Sievert's law.[18] While the concentration of dissolved oxygen in Fe at the interface with $Fe_{1-\delta}O$ is determined by the dissociation oxygen partial pressure of Wüstite. Hence, the mole fraction of dissolved oxygen in Fe at the surface ($N^s_{\underline{O}}$) and at the $Fe/Fe_{1-\delta}O$ interface ($N^e_{\underline{O}}$) reads:

$$\begin{aligned} N^s_{\underline{O}} &= Ks \times \sqrt{pO_2^{(\text{ambient})}} \\ N^e_{\underline{O}} &= Ks \times \sqrt{pO_2^{(\text{Fe/FeO})}}, \end{aligned} \quad [1]$$

where Ks is the Sievert's constant and $pO_2^{(\text{Fe/FeO})}$ is the dissociation oxygen partial pressure of Wüstite. The ambient oxygen partial pressure ($pO_2^{(\text{ambient})}$) as a function of temperature, hydrogen partial pressure, and dew point can be calculated from the data in Reference 19. Both Ks and $pO_2^{(\text{Fe/FeO})}$ are functions of temperature, namely:

$$Ks = \exp\left(\frac{-\Delta G^0_{\underline{O}}}{RT}\right), \quad [2]$$

and

$$pO_2^{(\text{Fe/FeO})} = \exp\left(\frac{2\Delta G^0_{\text{FeO}}}{RT}\right), \quad [3]$$

in which $\Delta G^0_{\underline{O}}$ is the standard free energy for O_2 dissolution in Fe, and ΔG^0_{FeO} is the standard free energy of reaction $Fe + 1/2O_2 = FeO$. Further, $\Delta G^0_{\underline{O}}$ and ΔG^0_{FeO} can be expressed in terms of enthalpy H, entropy S, and temperature T according to:

$$\Delta G^0_{\underline{O}} = \Delta H^0_{\underline{O}} - T\Delta S^0_{\underline{O}}, \quad [4]$$

and

$$\Delta G^0_{\text{FeO}} = \Delta H^0_{\text{FeO}} - T\Delta S^0_{\text{FeO}}, \quad [5]$$

respectively. Data of $\Delta G^0_{\underline{O}}$ can be evaluated from Reference 20, and ΔG^0_{FeO} is obtained from Reference 18.

Taking the concentration profile of dissolved oxygen in Fe linear, the flux of oxygen in the iron layer follows from Fick's first law:

$$J_{\underline{O}} = \frac{D_{\underline{O}}}{V_{m(\text{Fe})}} \frac{(N^e_{\underline{O}} - N^s_{\underline{O}})}{X}, \quad [6]$$

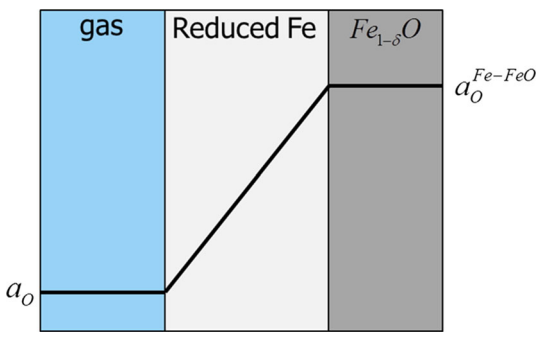

Fig. 1—Schematic presentation of oxygen activity profile across the iron layer during the steady-state reduction of a Wüstite scale.

where $V_{m(\mathrm{Fe})}$is the molar volume of Fe and X is the thickness of the reduced iron layer. $D_{\underline{\mathrm{O}}}$ is the bulk diffusion coefficient of oxygen in iron, which equals:

$$D_{\underline{\mathrm{O}}} = D^0_{\underline{\mathrm{O}}} \exp\left(\frac{-Q}{RT}\right) \quad [7]$$

Values of $D^0_{\underline{\mathrm{O}}}$ and Q are adopted from Reference 18. Since the growth rate of the reduced iron layer is coupled to the oxygen flux, it holds that:

$$\frac{dX}{dt} = J_{\underline{\mathrm{O}}}(1-\delta)V_{m(\mathrm{Fe})} \quad [8]$$

Integrating Eq. [8] gives:

$$X^2 = 2(1-\delta)D_{\underline{\mathrm{O}}}(N^e_{\underline{\mathrm{O}}} - N^s_{\underline{\mathrm{O}}})t \quad [9]$$

Usually, such a parabolic growth law is expressed as:

$$X^2 = 2kt, \quad [10]$$

where k is termed as the parabolic growth rate constant, which equals:

$$k = (1-\delta)D_{\underline{\mathrm{O}}}(N^e_{\underline{\mathrm{O}}} - N^s_{\underline{\mathrm{O}}}) \quad [11]$$

Alternatively, the kinetics of Wüstite reduction can be expressed in terms of the weight change per unit area as a function of square root of time, namely:

$$(\Delta m/S) = k_w t^{1/2} \quad [12]$$

For this parabolic growth rate constant, k_w can be written:

$$k_w = \frac{\sqrt{2}M_{\mathrm{O}}}{M_{\mathrm{Fe}}}\rho_{\mathrm{Fe}}[(1-\delta)D_{\underline{\mathrm{O}}}(N^e_{\underline{\mathrm{O}}} - N^s_{\underline{\mathrm{O}}})]^{1/2}, \quad [13]$$

in which M_{O} and M_{Fe} are the molar mass of oxygen and iron, respectively, and ρ_{Fe} is the density of iron, whose values are adopted from Reference 21. The value of δ in Wüstite at thermodynamic equilibrium with iron is typically about 0.05 from 873 K to 1273 K (600 °C to 1000 °C).[10] The value of k_w at different reduction temperatures and gas compositions (*i.e.,* dew points and hydrogen partial pressure) can then be predicted from Eq. [13]. When the ambient oxygen partial pressure is low (*e.g.*, low annealing dew point), $N^s_{\underline{\mathrm{O}}}$ is practically zero, and Eq. [13] can be simplified to:

$$k_w = \frac{\sqrt{2}M_{\mathrm{O}}}{M_{\mathrm{Fe}}}\rho_{\mathrm{Fe}}[(1-\delta)D_{\underline{\mathrm{O}}}N^e_{\underline{\mathrm{O}}}]^{1/2} \quad [14]$$

Combining Eqs. [1] through [5] and [7], the temperature dependence of k_w can be expressed as:

$$k_w = \frac{M_{\mathrm{O}}\rho_{\mathrm{Fe}}[2(1-\delta)D^0_{\underline{\mathrm{O}}}]^{1/2}}{M_{\mathrm{Fe}}} \times \exp\left(\frac{-\Delta S^0_{\underline{\mathrm{O}}} - \Delta S^0_{\mathrm{FeO}}}{2R}\right) \times \exp\left(\frac{-Q - \Delta H^0_{\underline{\mathrm{O}}} + \Delta H^0_{\mathrm{FeO}}}{2RT}\right) \quad [15]$$

Here, half the sum of $-Q$, $-\Delta H^0_{\underline{\mathrm{O}}}$, and $\Delta H^0_{\mathrm{FeO}}$ represents the activation energy of Wüstite reduction.

III. EXPERIMENTS AND METHODS OF INVESTIGATION

A. *Samples*

The Wüstite scale to study its reduction kinetics was created by oxidizing sheets of pure iron and a Mn alloyed steel in a gas mixture of Ar + 33 vol pct CO_2 + 17 vol pct CO. The chemical composition of the pure iron and the Mn alloyed steel is listed in Table I. Rectangular samples of 15 × 7 × 2 mm^3 for thermogravimetric analysis were cut from ingots by electric discharge machining (EDM). Also the Mn alloyed steel samples of 19 × 10 × 1 mm^3 were cut, but with a plate cutter from a cold-rolled sheet. All samples were grinded with SiC emery paper and then polished with 1 micron diamond grains. Between each preparation step, the samples were cleaned ultrasonically in isopropanol and dried by blowing with pure nitrogen (purity better than 5N). The dimension of each sample after preparation was measured with a caliper (accuracy ±0.05 mm). The samples were stored in airtight membrane boxes (Agar Scientific G3319, UK).

B. *Annealing*

A first series of oxidation and reduction experiments were performed with a symmetrical thermogravimetric analyzer (TGA, Setaram TAG 16/18, France). The sample was mounted onto a sapphire rod with an alumina pin having a diameter of 2.2 mm through a hole of diameter of 2.5 mm in the sample. A dummy sample of alumina with the same dimensions is mounted onto a sapphire rod of the counter part of the balance to eliminate any buoyancy effect.

The whole TGA system was pumped to vacuum (<50 Pa) and refilled with an Ar + 5 vol pct H_2 gas mixture twice to flush the gas lines, balance, and furnaces. Then the dual furnaces were heated up from room temperature to the target temperature with 5 K/min, while purging with 200 sccm Ar + 5 vol pct H_2, *i.e.,* 100 sccm gas in each furnace. When the target temperature for isothermal oxidation was reached, the gas composition was switched to Ar + 33 vol pct CO_2 + 17 vol pct CO while maintaining a total gas flow of 200 sccm. After oxidation, the conditions were switched to reduction either at the same temperature as for oxidation or at a specific temperature for isothermal reduction. The gas composition was switched to Ar + 5 or 10 vol pct H_2 while maintaining a total gas flow of 200 sccm. Finally, the furnace was cooled down to room temperature with 5 K/min, while keeping the gas composition the same as during reduction. Since no significant decarburization was observed during oxidation and reduction of Mn alloyed steels, the TG curves of the Mn steel during the reduction process represents the kinetics of Wüstite reduction.

A second series of experiments on the Mn alloyed steel samples were carried out in a horizontal quartz tube furnace (Carbolite MTF 12/38/850, UK) with an inner tube diameter of 30 mm. The sample was placed onto a quartz boat located at the cold zone of the

Table I. Chemical Composition of Iron and Mn Alloyed Steel as Determined by Optical Emission Spectrometry

	C (Wt. Pct)	Mn (Wt. Pct)	Si (Wt. Pct)	Al (Wt. Pct)	Ni (Wt. Pct)
Iron	0.002	—	0.003	0.040	0.005
Mn steel	0.103	1.70	0.049	0.002	—

furnace tube. Then the furnace was closed and flushed with pure Ar at a flow rate of 500 sccm. Next, the sample was moved to the hot zone of the furnace with a quartz rod. At the end of the annealing experiment the sample was moved in the reverse direction to the cold zone. The heating and cooling of the sample was relatively fast, about 140 to 180 K/min, respectively. The gas mixtures passed through the furnace tube at atmospheric pressure at a total flow rate of 500 sccm. The Mn alloyed steel samples were first oxidized in the Ar + 33 vol pct CO_2 + 17 vol pct CO gas mixture at 1223 K (950 °C) and then reduced in dry or wet Ar + 10 vol pct H_2 gas mixture at the same temperature. During reduction process the dew point was monitored with a cooled mirror analyzer (Optidew, Michell Instruments, UK). The fluctuation of dew points during reduction process was within ±2 K.

Prior to admitting the gas mixtures to any of the furnace, each gas, *i.e.*, Ar, H_2, CO_2, and CO (all with 5N vol pct purity), was filtered to remove any residual hydrocarbons, moisture, and oxygen, with Accosorb (<10 ppb hydrocarbons), Hydrosorb (<10 ppb H_2O), and Oxysorb (<5 ppb O_2) filters (Messer Griesheim, Germany), respectively. The flow of each gas was regulated and monitored using mass flow controllers (Bronkhorst, The Netherlands). To create a specific dew point in the furnace, de-aerated and deionized water (18.2 MΩ cm at 298 K (25 °C)) was evaporated with a gas line controlled evaporator mixer (CEM, Bronkhorst, The Netherlands). The pure water was de-aerated with nitrogen gas in a closed pressurized stainless steel vessel and the dissolved oxygen gas in the pure water is below 100 ppb, as measured with an O_2 sensor (InPro 6850i, METTLER TOLEDO). The partial pressure of evaporated H_2O in the Ar + H_2 gas mixture is related to dew point according to the formula given in Reference 19.

C. *Characterization*

X-ray diffraction (XRD) was used to identify the oxide phases formed after annealing. The XRD patterns were recorded with a Bruker D8 Advance diffractometer in the Bragg–Brentano geometry using Co Kα radiation, in the 2θ region between 10 deg and 110 deg with a step size of 0.034 deg 2θ and a dwell time of 2 s.

The surface and cross section of the annealed samples were examined with scanning electron microscopy (SEM) using a JSM6500F (JEOL, Japan) operated with an accelerating voltage of 5 or 15 kV. X-ray microanalysis (XMA) using Electron Dispersive Spectroscopy (EDS) was performed with the same SEM instrument equipped with an UltraDry 30 mm^2 detector (Thermo Fisher Scientific).

The concentration of Mn in the Wüstite formed on Mn alloyed steel as well as the Mn concentration in the iron layer formed after Wüstite reduction was determined with electron probe X-ray microanalysis (EPMA). The analysis was performed with a JXA 8900R (JEOL, Japan) microprobe employing Wavelength Dispersive Spectrometry (WDS). A focused electron beam was used with an energy of 10 keV and a current of 50 nA. All measurements were performed on the cross sections of samples. The composition at each analysis location of the sample was determined using the X-ray intensities of the constituent elements after background correction relative to the corresponding intensities of reference materials. In this case the X-ray intensities of Fe-Kα, Mn-Kα, and O-Kα were measured and pure Fe, Mn, and SiO_2, respectively, were used as references. The thus obtained intensity ratios were processed with a matrix correction program CITZAF.[22]

IV. RESULTS AND DISCUSSION

A. *Growth of Wüstite scale*

After oxidation of pure iron and Mn alloyed steel in the Ar + 33 vol pct CO_2 + 17 vol pct CO gas mixture, a dense oxide scale fully covering the surface was formed; see *e.g.*, Figure 2. According to XRD, the oxide scale on both pure iron and Mn steel is composed of Wüstite. However, the oxide scale on Mn steel contains Mn in solid solution, *i.e.,* $(Fe_{1-x}Mn_x)_{1-\delta}O$, as confirmed with EPMA. Mn is homogeneously distributed in the Wüstite scale on Mn steel with a concentration of about 3 at pct among metallic elements (*i.e., x* equals to 0.03 in $(Fe_{1-x}Mn_x)_{1-\delta}O$) after annealing in the Ar + 33 vol pct CO_2 + 17 vol pct CO gas mixture at 1223 K (950 °C) for 8 hours. An internal oxidation zone (IOZ) is formed beneath the Wüstite scale after oxidation of the Mn alloyed steel; see Figure 2(b). The oxide precipitates in the IOZ comprise (Mn,Fe)O with rock-salt crystal lattice.[23]

For both iron and the Mn alloyed steel, the Wüstite growth follows linear kinetics; see *e.g.,* Figures 3 and 4. This indicates that the level of oxygen partial pressure across the Wüstite scale is uniform and equals to the dissociation oxygen partial pressure of Wüstite.[24,25] Hence the composition of the Wüstite ($Fe_{1-\delta}O$ or $(Fe,Mn)_{1-\delta}O$) scale in terms of its metal deficiency δ equals to about 0.05.[10] The initial non-linear growth of Wüstite scale is due to stabilization of the flow and composition of the annealing gas atmosphere after switching to oxidation conditions, which takes about 20 to 30 minutes. Moreover, during the initial oxidation

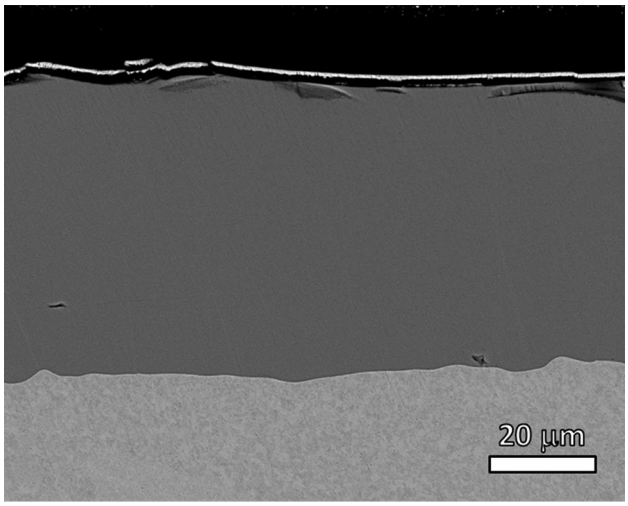

(a)

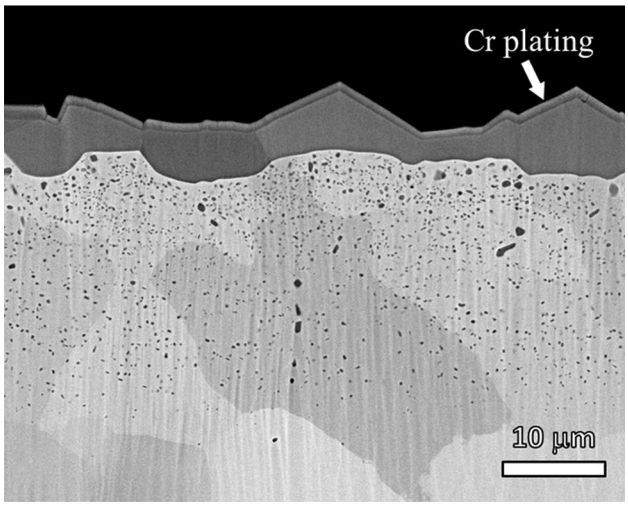

(b)

Fig. 2—SEM images (back scattered electrons) of cross section of a pure iron (*a*) and a Mn alloyed steel (*b*) after oxidizing at 1223 K (950 °C) in Ar + 33 vol pct CO_2 + 17 vol pct CO gas mixture for 3 and 8 h, respectively.

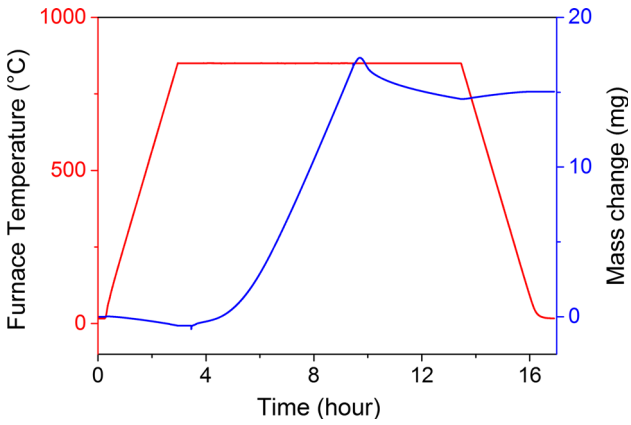

Fig. 3—Temperature profile and corresponding mass change of iron during first oxidation in Ar + 33 vol pct CO_2 + 17 vol pct CO gas mixture for 6 h and next reduction of the formed Wüstite in dry Ar + 5 vol pct H_2 gas mixture for 4 h both at 1123 K (850 °C).

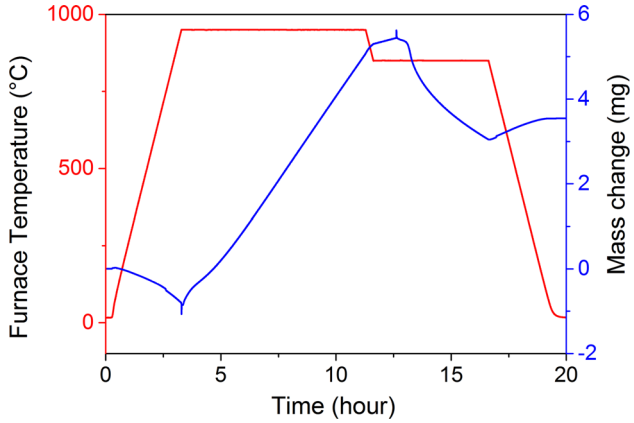

Fig. 4—Temperature profile and corresponding mass change curve of a Mn alloyed steel (cf. Table I) during first oxidation in Ar + 33 vol pct CO_2 + 17 vol pct CO gas mixture at 1223 K (950 °C) for 8 h and next at 1123 K (850 °C) for 1 h. Thereafter, the Wüstite layer on the Mn alloyed steel was reduced in dry Ar + 5 vol pct H_2 gas mixture for 4 h at 1123 K (850 °C).

stage the linear growth rate of Wüstite scale on pure iron in Ar + CO_2 + CO gas mixtures increases with time due to the evolution of the texture of the Wüstite scale.[26]

B. *Growth of Iron Layer*

When reducing the Wüstite scale, either formed on pure iron or on Mn alloyed steel, in an Ar + H_2 gas mixture, a dense and uniform layer of iron is formed beneath the surface. This iron layer separates the unreduced Wüstite scale from the reduction atmosphere; see *e.g.*, Figure 5. The iron layer is well adherent to the unreduced Wüstite scale. In contrast with results reported for the reduction of Wüstite in pure H_2 (see *e.g.,* Reference 27), no significant cracks or pores were observed in the iron layer nor at the scale–iron interface.

The lattice parameters of α-iron, γ-iron, and $Fe_{0.95}O$ at 1183 K (910 °C) are 0.2907, 0.3647, and 0.4363 nm, respectively.[28] Hence, reducing $Fe_{0.95}O$ to iron results in volume shrinkage of about 42 pct. However, the lattice misfit at the scale/iron interface can be much smaller. The orientation relationships at the iron/Wüstite interface is $(100)_{Fe}||(100)_{FeO}$ and $[010]_{Fe}||[011]_{FeO}$ for γ-iron , and $(100)_{Fe}||(100)_{FeO}$ and $[100]_{Fe}||[100]_{FeO}$ for γ-iron.[28,29] Then the misfit relative to the Wüstite lattice at iron/Wüstite interface is about 5.7 and 16.4 pct for α-iron and γ-iron , respectively. In addition, dissolved oxygen is normally considered to be present at the interstitial sites of iron lattice due to its similar diffusion coefficient as nitrogen and carbon in iron.[30] Hence, the outward flux of dissolved oxygen atoms to the surface does not lead to counter flux of vacancies to the iron/Wüstite interface. Therefore, good adhesion between iron and Wüstite scale is expected.

Reduction of FeO at 1223 K (950 °C) in Ar + 10 vol pct H_2 gas mixture occurs at dew points below 309 K (36 °C), while reduction of MnO at the same temperature requires dew points below 198 K (−75 °C). Thus, the MnO in the Wüstite scale formed on the Mn alloyed

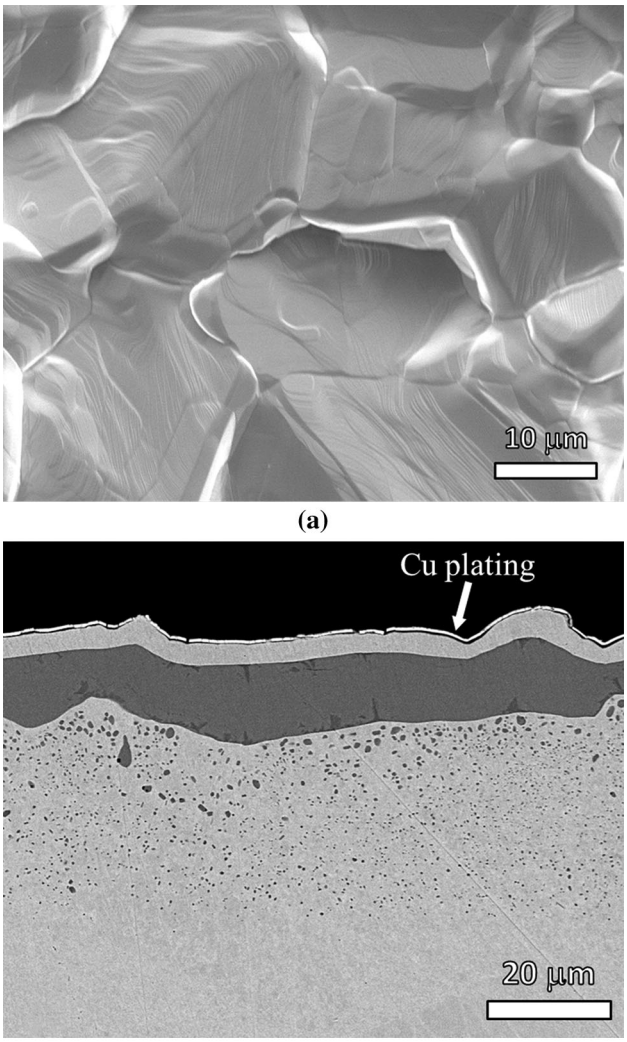

Fig. 5—SEM images (secondary electrons (*a*), back scattered electrons (*b*)) of surface (a) and cross section (b) of a Mn alloyed steel after first oxidizing at 1223 K (950 °C) for 8 h in Ar + 33 vol pct CO_2 + 17 vol pct CO gas mixture and next reducing at 1123 K (850 °C) for 4 h in Ar + 5 vol pct H_2 gas mixture.

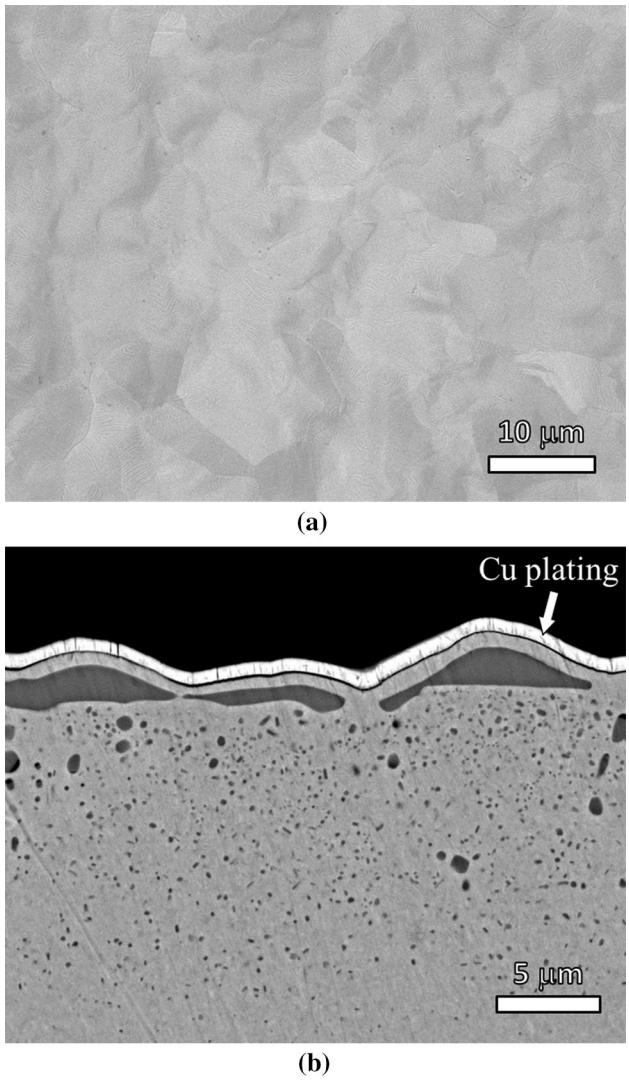

Fig. 6—SEM images (back scattered electrons) of surface (*a*) and cross section (*b*) of a Mn alloyed steel after first oxidizing in Ar + 33 vol pct CO_2 + 17 vol pct CO gas mixture for 3 h and then reducing in Ar + 10 vol pct H_2 gas mixture at dew point of 283 K (10 °C) for 15 min at constant temperature of 1223 K (950 °C).

steel will not be reduced in an Ar + H_2 gas mixture with a dew point of 10 °C. Nevertheless, an oxide-free surface of Mn alloyed steel is obtained by first forming and then reducing the Wüstite scale at 1223 K (950 °C). This is because the $(Fe,Mn)_{1-\delta}O$ scale dissociates into iron alone instead of iron plus embedded MnO particles. The Mn still remains in the unreduced $(Fe,Mn)_{1-\delta}O$ scale and the Mn concentration in the unreduced $(Fe,Mn)_{1-\delta}O$ scale increases with reduction time. Apparently, transport of Mn occurs towards the remaining Wüstite. Figure 6 shows the surface and cross section of the Mn steel after, first oxidizing at 1223 K (950 °C) for 3 hours in Ar + 33 vol pct CO_2 + 17 vol pct CO gas mixture and then reducing at same temperature for 15 minutes in Ar + 10 vol pct H_2 gas mixture at dew point of 283 K (10 °C), and no external MnO was observed. After reducing for 2.5 hours with the same annealing parameters, the Wüstite scale formed during the oxidation stage can be fully reduced; see Figure 7. The iron layer formed after the reduction of Wüstite scale is well adhered to the original steel matrix. The Mn concentration in the formed iron layer is practically zero. However, the Mn concentration in the remaining Wüstite scale increases with reduction time (x in $(Fe_{1-x}Mn_x)_{1-\delta}O$ increases from 0.03 to 0.07 after 15 minutes of reduction). After full reduction of the oxide scale, the small amount of Mn dissolved in the Wüstite turns into internal (Mn,Fe)O precipitates underneath the surface; see Figure 7(b).

C. *Kinetics of Wüstite Reduction*

The reduction kinetics of the Wüstite layer by hydrogen can be predicted using Eq. [15] with the data summarized in Table II. The temperature dependence of the parabolic rate constant is dominated by the temperature dependence of the oxygen diffusivity in iron. The

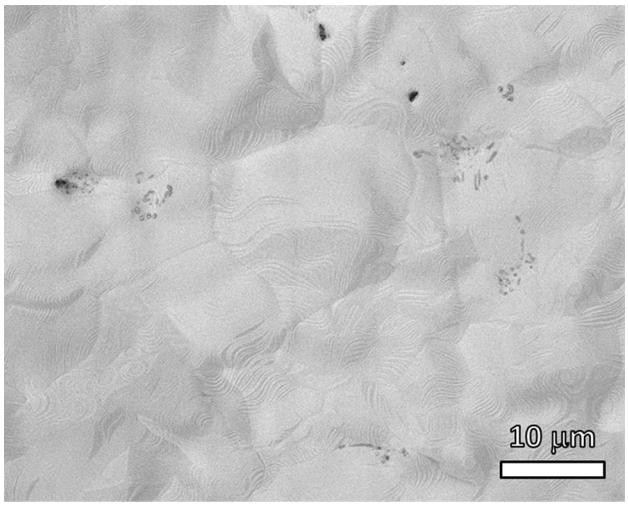

(a)

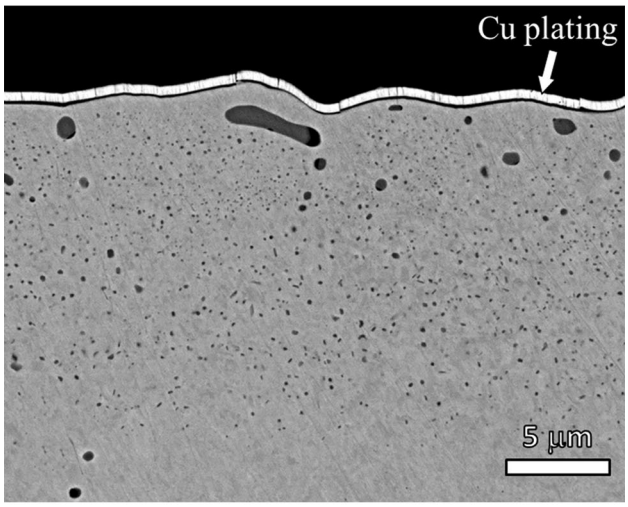

(b)

Fig. 7—SEM images (back scattered electrons) of surface (*a*) and cross section (*b*) of a Mn alloyed steel after first oxidizing in Ar + 33 vol pct CO_2 + 17 vol pct CO gas mixture for 3 h and then reducing in Ar + 10 vol pct H_2 gas mixture at dew point of 283 K (10 °C) for 2.5 h at constant temperature of 1223 K (950 °C).

activation energy for Wüstite reduction predicted using Eq. [15] is 104 kJ/mol if the formed iron layer is in the ferrite phase, while the activation energy for oxygen diffusion in ferrite equals 98 kJ/mol.[18] The parabolic rate constant for Wüstite reduction as a function of temperature in dry reducing atmosphere is presented in Figure 8. The parabolic rate constant of Wüstite reduction is determined experimentally with the approach illustrated in the Appendix to this paper. Comparison of these predicted values with experimentally determined parabolic rate constants for the reduction of Wüstite on both pure iron and the Mn alloyed steel shows good agreement; see Figure 8. This suggests that the kinetics of Wüstite reduction at steady state in Ar + H_2 gas mixture is indeed controlled by the bulk diffusion of dissolved oxygen in the formed iron layer. Also it confirms that the rate of oxygen take-up by hydrogen at iron surface and the decomposition of Wüstite at

Table II. Summary of the Data Adopted for Calculation of Parabolic Rate Constant for Wüstite Reduction

Parameters	Values	References
$D_{\underline{O}}^{0}(\alpha)$ ($cm^2\ s^{-1}$)	0.037	18
$Q(\alpha)$ ($J\ mol^{-1}$)	98000	18
$D_{\underline{O}}^{0}(\gamma)$ ($cm^2\ s^{-1}$)	5.75	18
$Q(\gamma)$ ($J\ mol^{-1}$)	168000	18
$\Delta H_{\underline{O}}^{0}(\alpha)$ ($J\ mol^{-1}$)	−154834	20
$\Delta S_{\underline{O}}^{0}(\alpha)$ ($J\ mol^{-1}\ K^{-1}$)	−70.3	20
$\Delta H_{\underline{O}}^{0}(\gamma)$ ($J\ mol^{-1}$)	−173021	20
$\Delta S_{\underline{O}}^{0}(\gamma)$ ($J\ mol^{-1}\ K^{-1}$)	−86.5	20
ΔH_{FeO}^{0} ($J\ mol^{-1}$)	−264890	18
ΔS_{FeO}^{0} ($J\ mol^{-1}\ K^{-1}$)	−65.4	18
ρ_{Fe} ($g\ cm^{-3}$)	7.9	21
M_{Fe} ($g\ mol^{-1}$)	56	21
M_O ($g\ mol^{-1}$)	16	21

scale–alloy interface are fast compared with the oxygen transport in the iron layer. Moreover, it suggests that the adopted data of oxygen diffusion in iron[18] as well as oxygen dissolution in iron[20] are valid.

Since the diffusion coefficient of oxygen for ferrite is much larger than for austenite,[18] the parabolic rate constant for Wüstite reduction suddenly drops due to the phase transformation of iron from ferrite into austenite. Hence, the reduction of Wüstite is relatively faster when the formed iron layer is ferrite rather than austenite. Moreover, the Sievert's constant for oxygen dissolution in ferrite is slightly higher than that in austenite,[20] which also contributes to the decrease of the parabolic rate constant (see Eqs. [1] and [14]) when the iron layer transforms from ferrite into austenite. This is in agreement with the experimental results that the observed parabolic rate constants for the reduction of Wüstite on pure iron and Mn alloyed steel at 1223 K (950 °C) (*i.e.*, both in austenite state) are much lower than those predicted for a ferrite layer; see Figure 8.

The kinetics of Wüstite reduction also depends on the oxygen partial pressure in the gas phase, which is related to dew point and H_2 partial pressure.[19] Increasing the oxygen partial pressure in the reduction atmosphere, increases the concentration of dissolved oxygen at the iron surface ($N_{\underline{O}}^{s}$) and thus reduces the parabolic rate constant for Wüstite reduction; see Eq. [13]. As can be seen in Figure 9, at 1123 K (850 °C) the parabolic rate constant for Wüstite reduction is practically independent of oxygen partial pressures up to 3×10^{-20} atm, but decreases rapidly at higher oxygen partial pressures. At the dissociation oxygen partial pressure of Wüstite the reduction process does not take place and hence the parabolic rate constant for Wüstite reduction drops to zero. However, in an annealing atmosphere with a dew point lower than 283 K (10 °C) and a H_2 volume fraction larger than 5 pct, the effect of oxygen partial pressure on the parabolic rate constant for Wüstite reduction is small compared with the effect of temperature.

The dissolution of Mn in the Wüstite scale with a concentration of 3 at. pct may lower the parabolic rate constant for Wüstite reduction by about 1.7 pct (cf. Eqs. [1] and [14]), which is relatively small and neglected in this study. The dissociation oxygen partial pressure at the interface between iron layer and Wüstite scale decreases with Mn concentration in the Wüstite scale, because the activity of FeO in the (Fe,Mn)O solution is less than unity.

The dissociation of Wüstite scale occurs not only at the scale/iron interface, but also at the original steel/scale interface, because the oxygen activity in the steel is lower than the dissociation oxygen partial pressure of Wüstite. The predicted and measured parabolic rate constants shown in Figures 8 and 9 only reflect the reduction process at scale/iron interface, since the reduction at steel/scale interface does not result in any weight change of sample. Hence, the total reduction rate of the Wüstite scale is higher than that determined from the measured mass loss. However, the amount of Wüstite reduced at the scale/steel interface is small compared with that at the scale/iron interface. The Wüstite dissociation at the steel/scale interface provides the oxygen source that allows inward oxygen diffusion and thus forms an internal oxidation zone (IOZ) beneath the Wüstite scale; see *e.g.*, Figures 2 and 5. The rate of Wüstite dissociation at scale/steel interface equals to the flux of oxygen into the IOZ, and thus can be estimated from the kinetics of internal oxidation underneath the Wüstite scale. The gradient of dissolved oxygen in the IOZ is almost linear,[18,31] and the flux of oxygen into the steel at the steel/scale interface can thus be estimated with Fick's 1st law. Since the levels of the oxygen partial pressure at steel/scale and scale/iron interfaces are almost the same and the oxygen concentration at the IOZ front equals zero, the ratio of the

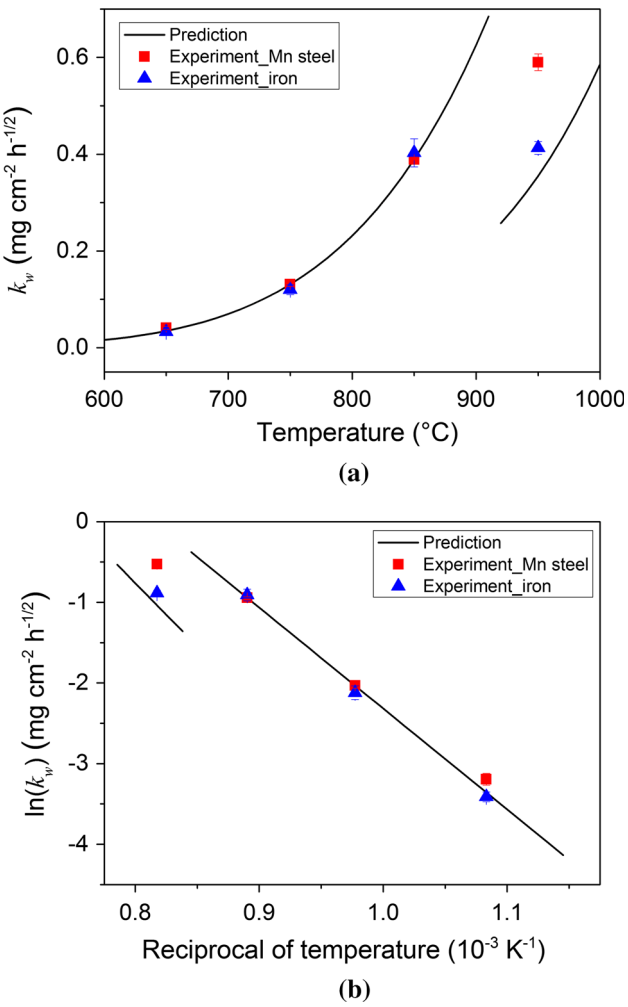

Fig. 8—Comparison between the predicted (cf. Eq. [13]) and experimentally determined parabolic reduction constants of Wüstite on pure iron and a Mn alloyed steel alloy at different temperatures; normal plot (*a*) and Arrhenius plot (*b*). The formed iron layer is in ferritic phase below 1185 K (912 °C) and in austenitic phase above 1185 K (912 °C). Note that the oxygen concentration at the reduced iron/gas interface was taken zero, *i.e.*, $N_{\underline{O}}^{s} = 0$.

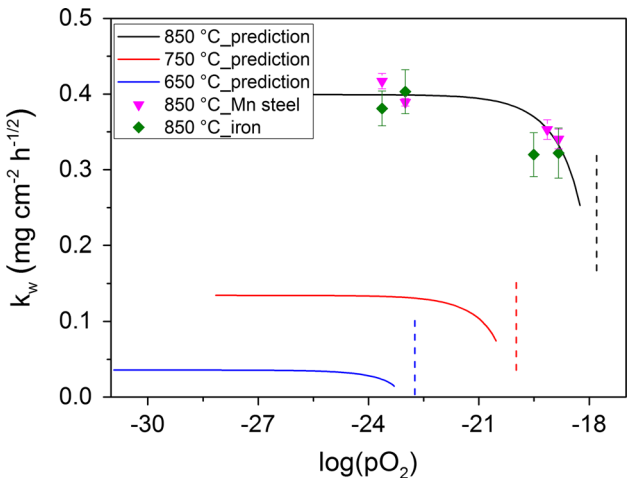

Fig. 9—Effect of oxygen partial pressure on parabolic rate constant of Wüstite reduction at temperatures of 923 K, 1023 K, and 1123 K (650 °C, 750 °C, and 850 °C). Dashed lines indicate the dissociation oxygen partial pressure of Wüstite. Note that the oxygen partial pressure in dry Ar + H_2 gas mixture is calculated assuming a dew point of 228 K (−45 °C).

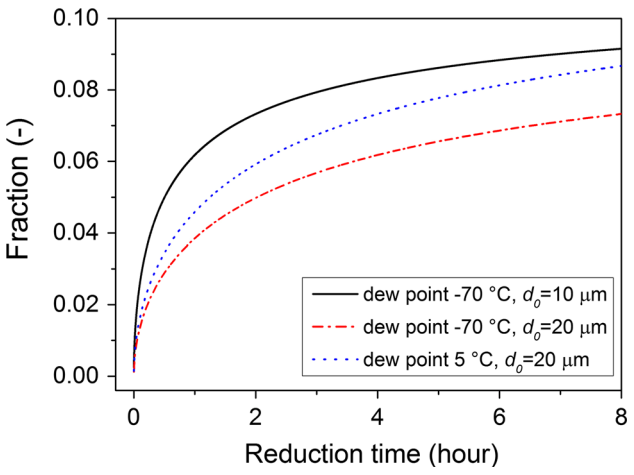

Fig. 10—Fraction of Wüstite reduced at scale/steel interface at 1123 K (850 °C) in Ar + 5 vol pct H_2 gas mixture with dew point of 203 K or 278 K (−70 °C or 5 °C). At the beginning of the reduction process, the depth of IOZ equals d_0.

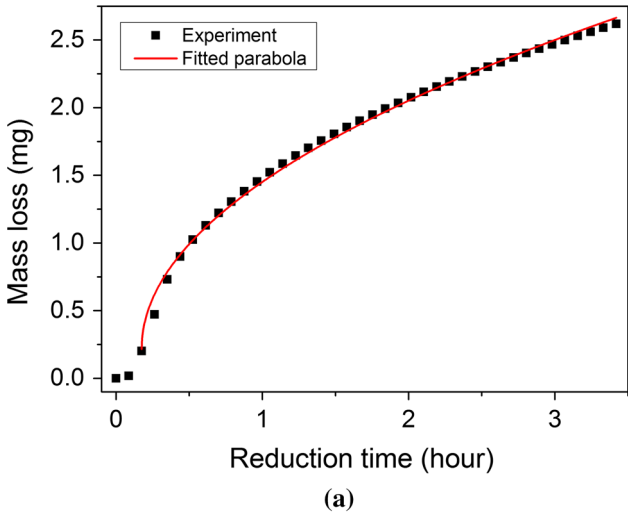

Fig. A1—Mass change during the reduction in dry Ar + 5 vol pct H_2 gas mixture at 1123 K (850 °C) of Wüstite on pure iron (*a*) and on a Mn alloyed steel (*b*). A parabolic rate law was fitted to the data (cf. Eq. [A1]).

Wüstite reduction rate at scale/iron interface over that at scale/steel interface can be estimated with:

$$\frac{J_{\underline{O}}^{FeO/Fe}}{J_{\underline{O}}^{FeO/steel}} = \frac{N_{\underline{O}}^{e} - N_{\underline{O}}^{s}}{N_{\underline{O}}^{e}} \frac{d}{X} \qquad [16]$$

where d is the depth of IOZ underneath the Wüstite scale, $J_{\underline{O}}^{FeO/Fe}$ and $J_{\underline{O}}^{FeO/steel}$ represent the oxygen flux from Wüstite to the iron layer and from Wüstite to the steel substrate, respectively. The increase of the depth of IOZ (d) during the reduction process can be estimated from the classical internal oxidation theory.[18] The thickness of the iron layer (X) as a function of reduction time can be calculated using Eq. [4]. The ratio of the amount of Wüstite reduced at scale/iron interface over the amount of Wüstite reduced at scale/steel interface equals to the ratio of the integration of the oxygen flux at the two interfaces, *i.e.*, $\int J_{\underline{O}}^{FeO/Fe} dt / \int J_{\underline{O}}^{FeO/steel} dt$. Figure 10 shows the predicted fraction of the amount of Wüstite scale reduced at the scale/steel interface as a function of reduction time. The depth of IOZ before the start of reduction process was taken 10 or 20 μm. The dew point in the reducing atmosphere was taken 203 K and 278 K (−70 °C and 5 °C). Although the fraction of the amount of Wüstite reduced at the scale/steel interface increases with reduction time, the dominant reduction process of Wüstite scale occurs at the scale/iron interface. For example, after oxidizing the Mn alloyed steel at 1223 K (950 °C) for 8 hours and then reducing in dry Ar + 5 vol pct H_2 gas mixture at 1123 K (850 °C) for 4 hours, the contribution of the amount of Wüstite reduced at the scale/steel interface to the total amount of Wüstite reduced is about 6 pct. Thus, the calculated reduction kinetics of the scale/iron interface (see Section II) provides a satisfactory estimate on the total reduction kinetics of the Wüstite scale.

V. CONCLUSIONS

Oxidizing pure iron and Mn alloyed steel in Ar + 33 vol pct CO_2 + 17 vol pct CO gas mixture forms a dense Wüstite scale. A dense and uniform layer of pure iron is formed at the surface of the Wüstite scale after reduction in Ar + H_2 gas mixtures. The reduction of the Wüstite scale follows a parabolic rate law at steady state. The parabolic rate constant of Wüstite reduction for Wüstite grown onto pure iron and the Mn steel is the same. The kinetics of Wüstite reduction in Ar + H_2 gas mixtures is controlled by bulk diffusion of dissolved oxygen in the formed Fe layer. Mn is dissolved in the Wüstite scale formed during oxidation of Mn alloyed steel. Mn remains dissolved in unreduced Wüstite scale during reduction process. An oxide-free surface of Mn alloyed steel can be obtained by forming first a Wüstite scale that subsequently is reduced in a Ar + H_2 gas mixture.

ACKNOWLEDGMENTS

This research was carried out under project number M22.3.11439 in the framework of the research program of the Materials innovation institute (M2i). Financial support from International Zinc Association (IZA) for program ZCO-62 is gratefully acknowledged. The authors are indebted to Dr. W. Melfo of Tata Steel (IJmuiden, The Netherlands) for providing the Mn alloyed steels and the composition analysis. The authors are also indebted to Ing. J.C. Brouwer and Ing. C. Kwakernaak for technical support and assistance with experiments.

APPENDIX: DETERMINATION OF STEADY-STATE PARABOLIC RATE CONSTANT

The reduction kinetics of Wüstite in terms of the steady-state parabolic rate constant is determined from the mass change observed with TGA; see Section III. First a Wüstite layer was formed by oxidizing in Ar + 33 vol pct CO_2 + 17 vol pct CO gas mixture and next this layer was reduced by switching the gas atmosphere to Ar + H_2. Since purging of the reducing gas mixture takes time, the initial stages of Wüstite reduction cannot be captured. Hence, in order to obtain a value for the steady-state parabolic rate constant, the observed reduction kinetics was fitted with:

$$y = A(x - x_0)^{0.5} + y_0 \qquad [A1]$$

where A, x_0, and y_0 (representing the imaginary starting point of steady-state reduction kinetics) are unknown and were obtained after fitting, x and y represent the reduction time and mass loss, respectively. The value obtained for the coefficient A is the effective parabolic constant for Wüstite reduction. As an example, Figure A1 shows the TG curve during the reduction of Wüstite scale for both pure iron and the Mn alloyed steel samples at 1123 K (850 °C) as well as the corresponding least-square fitted parabolic curve. The error in the determination of the effective parabolic constant was estimated by varying the range of data selected for the fitting.

REFERENCES

1. N. Fonstein: *Advanced High Strength Sheet Steels*, Springer International Publishing, Switzerland, 2015, p. 7.
2. A.R. Marder: *Prog. Mater. Sci.*, 2000, vol. 45, pp. 191–271.
3. G.M. Song, T. Vystavel, N. van der Pers, J.T.M. De Hosson, and W.G. Sloof: *Acta Mater.*, 2012, vol. 60, pp. 2973–81.
4. E.M. Bellhouse and J.R. McDermid: *Metall. Mater. Trans. A*, 2010, vol. 41, pp. 1539–53.
5. H. Liu, Y. He, S. Swaminathan, M. Rohwerder, and L. Li: *Surf. Coat. Tech.*, 2011, vol. 206, pp. 1237–43.
6. V.A. Lashgari, C. Kwakernaak, and W.G. Sloof: *Oxid. Met.*, 2014, vol. 81, pp. 435–51.
7. M. Blumenau, C.O. Gusek, M. Norden and R. Schonenberg: *2012 AISTech Conference Proceedings*, AIST, 2012.
8. W. Liu, J.Y. Lim, M.A. Saucedo, A.N. Hayhurst, S.A. Scott, and J.S. Dennis: *Chem. Eng. Sci.*, 2014, vol. 120, pp. 149–66.
9. P.C. Hayes: *Metall. Trans. B*, 1979, vol. 10, pp. 211–17.
10. R.A. Giddings and R.S. Gordon: *J. Am. Ceram. Soc.*, 1973, vol. 56, pp. 111–16.
11. D.H. St, S.P.Matthew. John, and P.C. Hayes: *Metall. Trans. B*, 1984, vol. 15, pp. 709–17.
12. A.M. Watts, D.H. St. John, and P.C. Hayes: John and P.C. Hayes*Metall. Trans. B*, 1983, vol. 14, pp. 753–59.
13. M. Farren, S.P. Matthew, and P.C. Hayes: *Metall. Trans. B*, 1990, vol. 21, pp. 135–39.
14. E.T. Turkdoga and J.V. Vinters: *Metall. Trans.*, 1972, vol. 3, pp. 1561–74.
15. P.C. Hayes: *Steel Res. Int.*, 2011, vol. 82, pp. 480–93.
16. H.K. Kohl and H.J. Engell: *Arch. Eisenhüttenwes.*, 1963, vol. 34, pp. 411–18.
17. L. von Bogdandy and H.J. Engell: *The Reduction of Iron Ores*, Springer, Berlin Heidelberg, Berlin, 1976, pp. 133–34.
18. D.J. Young: *High Temperature Oxidation and Corrosion of Metals*, Elsevier, Oxford, 2008, pp. 33, 46, 258, 565.
19. D. Huin, P. Flauder, and J.B. Leblond: *Oxid. Met.*, 2005, vol. 64, pp. 131–67.
20. V.A. Lashgari: Ph.D Dissertation, Delft University of Technology, 2014, pp. 128.
21. D.R. Lide: *CRC Handbook of Chemistry and Physics*, 88th ed., Taylor & Francis, Florida, 2007.
22. J.T. Armstrong: *Electron Probe Quantitation*, Springer, US, Boston, 1991, pp. 261–315.
23. W. Mao and W.G. Sloof: *Scr. Mater.*, 2017, vol. 135, pp. 29–32.
24. F.S. Pettit and J.B. Wagner, Jr: *Acta Metall.*, 1964, vol. 12, pp. 35–40.
25. R. Bredesen and P. Kofstad: *Oxid. Met.*, 1991, vol. 36, pp. 27–56.
26. R. Bredesen and P. Kofstad: *Oxid. Met.*, 1990, vol. 34, pp. 361–79.
27. D.H. St. John and P.C. Hayes: *Metall. Trans. B*, 1982, vol. 13, pp. 117–24.
28. D.H. St, S.P.Matthew. John, and P.C. Hayes: *Metall. Trans. B*, 1984, vol. 15, pp. 701–08.
29. Y. Sasaki, M. Bahgat, M. Iguchi, and K. Ishii: *ISIJ Int.*, 2005, vol. 45, pp. 1077–83.
30. C. Wagner: *Acta Metall.*, 1973, vol. 21, pp. 1297–303.
31. V.A. Lashgari, G. Zimbitas, C. Kwakernaak, and W.G. Sloof: *Oxid. Met.*, 2014, vol. 82, pp. 249–69.